A junctional cAMP compartment regulates rapid Ca^{2+} signaling in atrial myocytes

Full Length Article

Sören Brandenburg[1,2,3] ✉, Jan Pawlowitz[1], Vanessa Steckmeister[4], Hariharan Subramanian[5], Dennis Uhlenkamp[1], Marina Scardigli[6,7], Mufassra Mushtaq[1], Saskia I. Amlaz[1,3], Tobias Kohl[1,3], Jörg W. Wegener[1,3], Demetrios A. Arvanitis[8], Despina Sanoudou[8], Leonardo Sacconi[7,9], Gerd Hasenfuß[1,2,3], Niels Voigt[2,3,4], Viacheslav O. Nikolaev[5,10], Stephan E. Lehnart[1,2,3,11] ✉

[1] Cellular Biophysics and Translational Cardiology Section, Department of Cardiology & Pneumology, Heart Research Center Göttingen, University Medical Center Göttingen, Göttingen, Germany. [2] DZHK (German Centre for Cardiovascular Research), partner site Göttingen, Germany. [3] Cluster of Excellence "Multiscale Bioimaging: from Molecular Machines to Networks of Excitable Cells" (MBExC), University of Göttingen, Germany. [4] Institute of Pharmacology and Toxicology, Heart Research Center Göttingen, University Medical Center Göttingen, Göttingen, Germany. [5] Institute of Experimental Cardiovascular Research, University Medical Center Hamburg-Eppendorf, Hamburg, Germany. [6] Department of Physics and Astronomy, University of Florence, Florence, Italy. [7] European Laboratory for Non-Linear Spectroscopy and National Institute of Optics (INO-CNR), Sesto Fiorentino, Italy. [8] Molecular Biology Division, Biomedical Research Foundation, Academy of Athens, Athens, Greece. [9] Institute for Experimental Cardiovascular Medicine, University Heart Center Freiburg, Faculty of Medicine, University of Freiburg, Freiburg im Breisgau, Germany. [10] DZHK (German Centre for Cardiovascular Research), partner site Hamburg/Kiel/Lübeck, Germany. [11] BioMET, Center for Biomedical Engineering and Technology, University of Maryland School of Medicine, Baltimore, Maryland, USA.

✉ Corresponding authors: Sören Brandenburg and Stephan E. Lehnart

University Medical Center Göttingen; Robert-Koch-Str. 42a, 37075 Göttingen, Germany

Tel: +49 551 39-63637; Email: soeren.brandenburg@med.uni-goettingen.de

Supplementary Material

1. Supplementary Figures and Figure Legends
2. Supplementary Tables
3. Supplementary Methods

Supplementary Figure 1. STED imaging point spread function and *in situ* resolution.

Supplementary Figure 2. Full scans of Western blots presented in the main manuscript figures.

Supplementary Figure 3. Full scans of Western blots presented in the supplementary figures.

Supplementary Figure 4. Aspartyl/asparaginyl β-hydroxylase (ASPH) protein expression in mouse cardiac tissue lysates.

Supplementary Figure 5. Specificity control of the primary junctin and RyR2-pS2808 antibodies in isolated cardiomyocytes.

Supplementary Figure 6. Preserved RyR2 clustering in *Asph*$^{-/-}$ atrial myocytes.

Supplementary Figure 7. Preserved expression of Ca^{2+} handling proteins in Epac1-JNC transgenic atria.

Supplementary Figure 8. Coimmunoprecipitation of transgenic Epac1-JNC and endogenous JNC by RyR2 in atrial tissue lysates.

Supplementary Figure 9. Confocal imaging and 3D reconstruction of the TAT network throughout a living atrial myocyte volume confirming abundant axial tubules connected to the surface membrane through transverse tubule components.

Supplementary Figure 10. Confirmation of preserved TAT network components in Epac1-JCN transgenic atrial myocytes.

Supplementary Figure 11. Confocal and STED imaging resolution of individual Epac1-JNC clusters in living atrial myocytes.

Supplementary Figure 12. Subsurface versus TAT-associated RyR2 clusters show similar Epac1-JNC/RyR2 signal ratios.

Supplementary Figure 13. Phospho-epitope specific immunofluorescence imaging confirming highly phosphorylated junctional RyR2 clusters in an Epac1-JNC transgenic atrial myocyte.

Supplementary Figure 14. Epifluorescence cAMP FRET imaging and correction of CFP bleedthrough for confocal FRET imaging.

Supplementary Figure 15. Inducible PKA-mediated RyR2 phosphorylation at Ser2808 upon β-adrenergic stimulation.

Supplementary Figure 16. The adenylyl cyclase inhibitors NKY80 and SQ22,536 do not significantly affect the pS2808/RyR2 phosphorylation ratio.

Supplementary Figure 17. Diastolic intracellular Ca^{2+} increase following MDL treatment.

Supplementary Figure 18. Adenylyl cyclase inhibition delays action potential time-to-peak and duration.

Supplementary Figure 19. Time course of the L-type Ca^{2+} current density after MDL application.

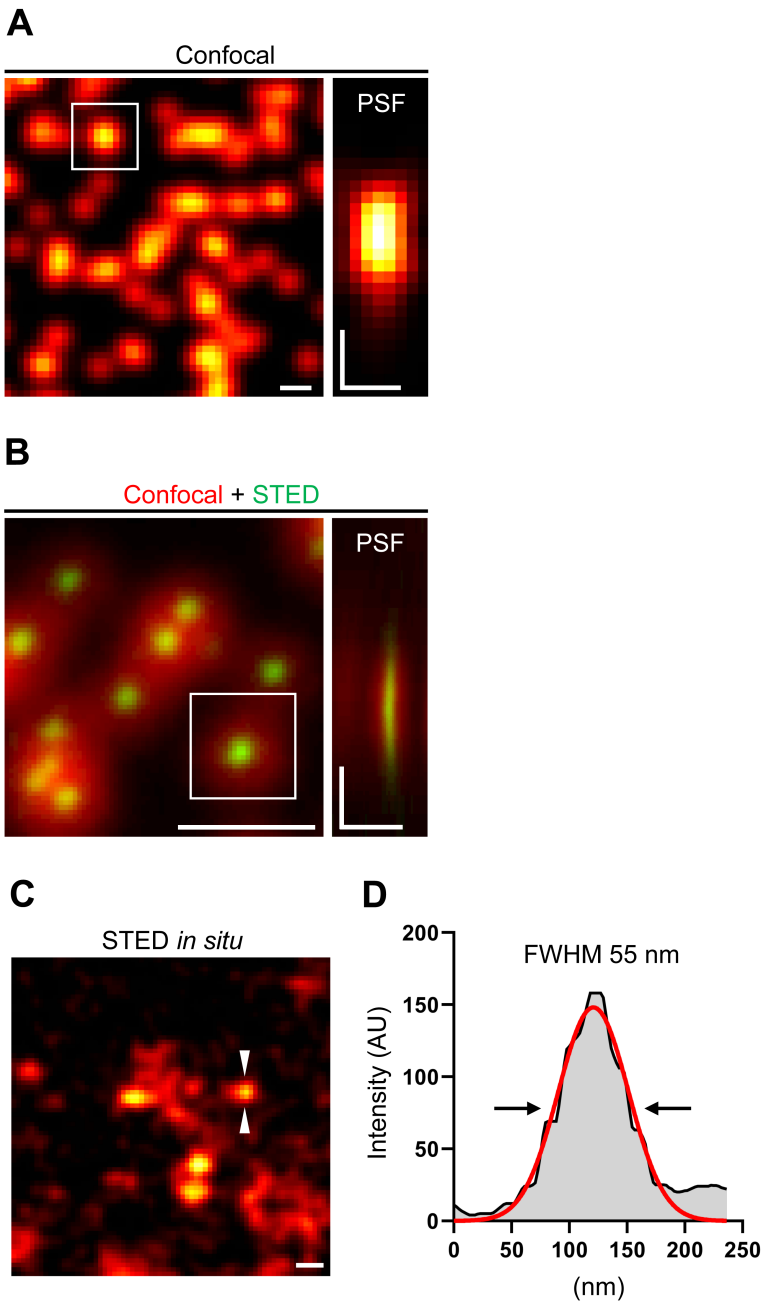

Supplementary Figure 1. STED imaging point spread function and *in situ* resolution. (**A**) Confocal nanobead (Nanoparticles red fluorescent 40 nm, Abberior Instruments) imaging (Zeiss LSM 880, Plan-Apochromat 63x/1.40 oil objective). The 40 nm nanobeads were confocally detected with a FWHM of 330.0 nm ± 5.9 nm (n = 7). 100 nm lateral pixel size; scale bars 500 nm. (**B**) Confocal (*red*) followed by STED (*green*) imaging (Leica TCS-SP8, HC PL APO C2S 100x/1.40 oil objective) of the same 40 nm sized nanobeads described in **A**. The left image superposition showed the increased lateral resolution of STED as green signal spots versus confocal imaging generating blurred red signals. Here, the 40 nm nanobeads were detected with a FWHM of 70.2 ± 6.4 nm in STED imaging (n = 7). 16 nm lateral pixel size; scale bars 500 nm. The white box indicates the signal spot magnified as xz point spread function (PSF) in **A** and **B**. (**C**) Magnified region-of-interest from a STED image of an Epac1-JNC transgenic atrial myocyte showing the raw anti-YFP immunostained intracellular signals. Scale bar 100 nm. White arrowheads indicate a laterally resolved signal spot, which was analyzed in **D**. (**D**) Signal intensity distribution plot (*black trace*) and Gaussian fit (*red trace*). Horizontal arrows indicate the calculated FWHM = 55 nm as an estimate of the *in situ* STED imaging resolution in fixed AMs.

Figure 1A

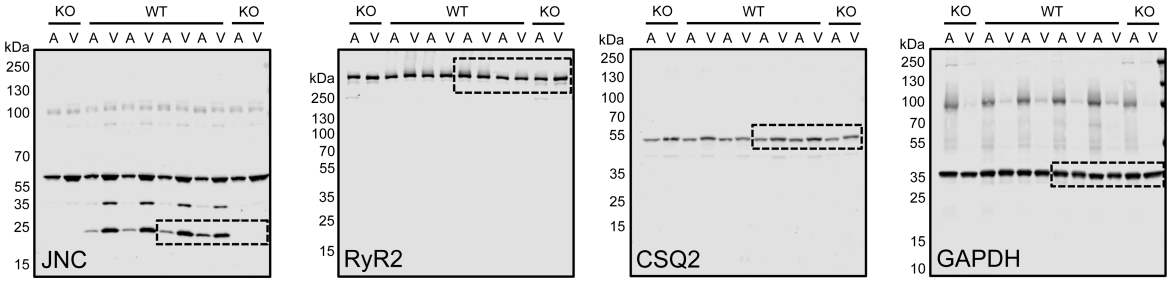

Figure 2A

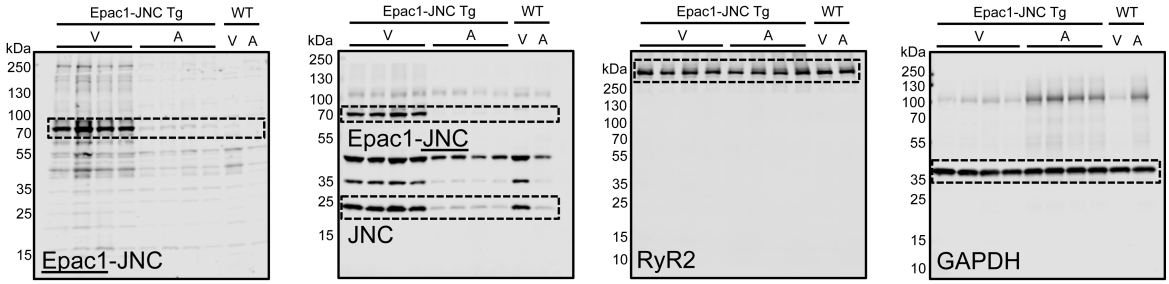

Figure 5E

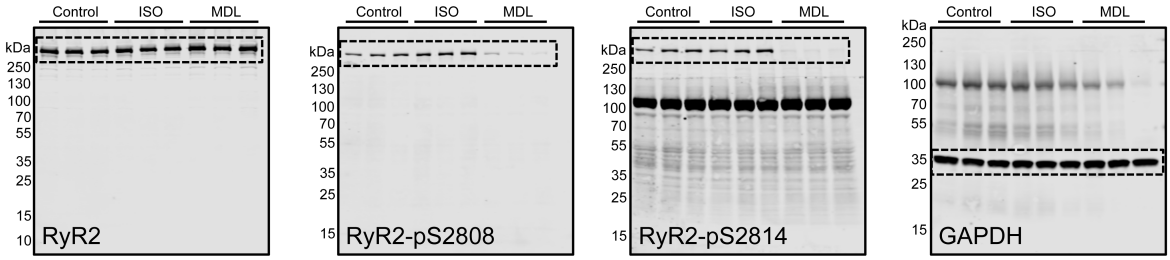

Supplementary Figure 2. Full scans of Western blots presented in the main manuscript figures. Dashed frames indicate the data shown in the main manuscript figures.

Supplemental Figure 4

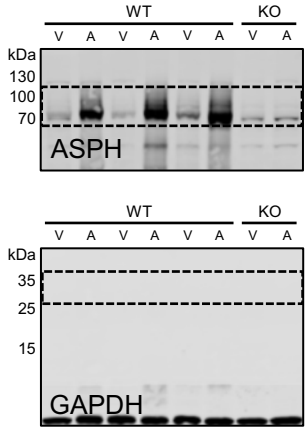

Supplemental Figure 8

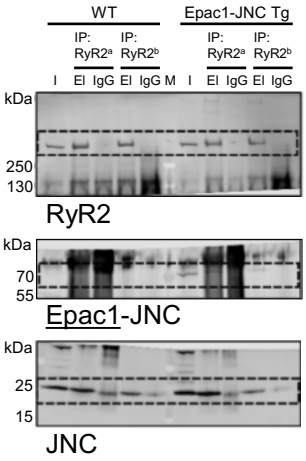

Supplemental Figure 7

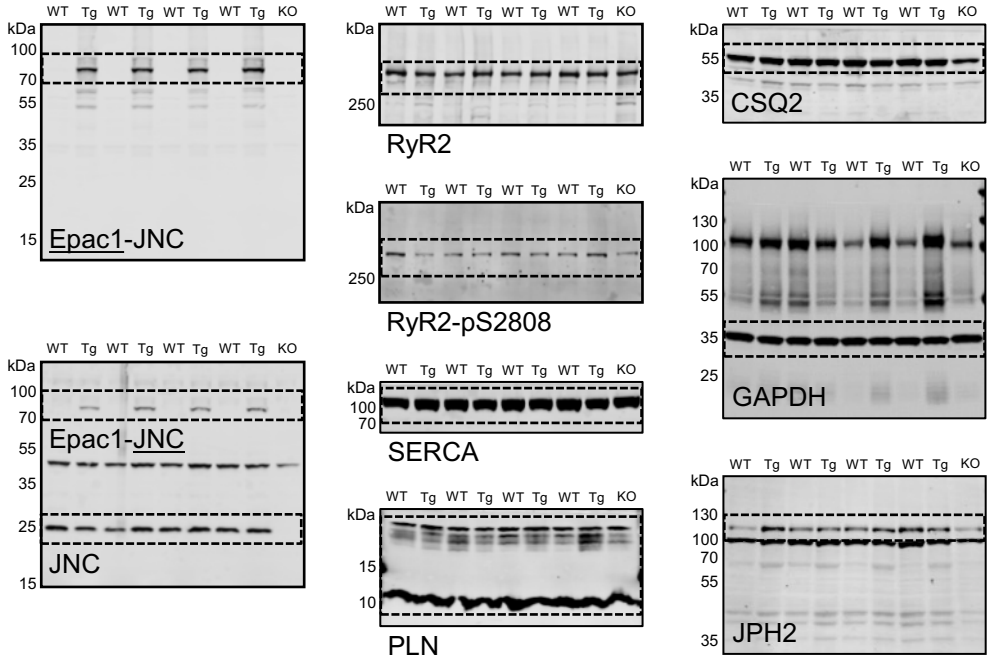

Supplemental Figure 15

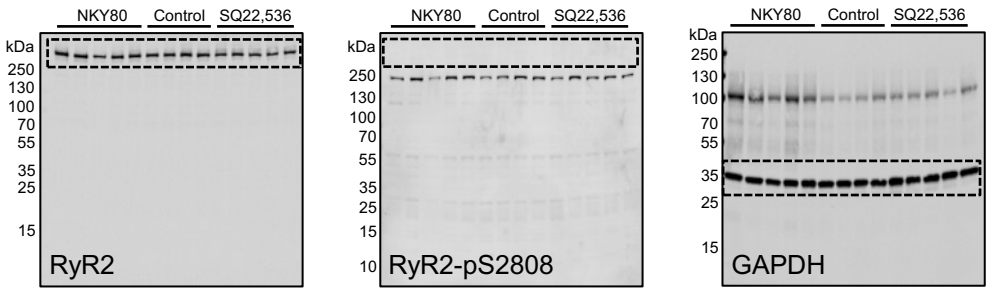

Supplementary Figure 3. Full scans of Western blots presented in the supplementary figures. Dashed frames indicate the cropped data shown in the supplementary figures.

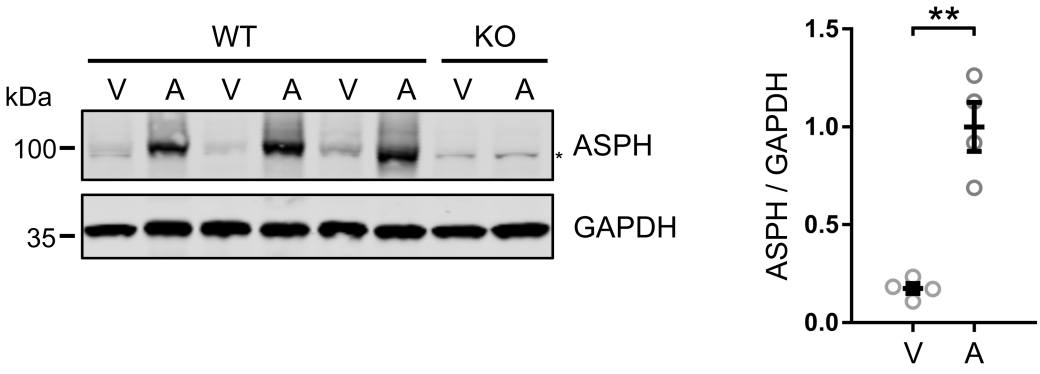

Supplementary Figure 4. Aspartyl/asparaginyl β-hydroxylase (ASPH) protein expression in mouse cardiac tissue lysates. (**A**) Immunoblotting of cardiac lysates from wild-type (WT) and *Asph*$^{-/-}$ (KO) mice showing significantly higher ASPH expression levels in paired atrial (A) compared to ventricular (V) tissues. Asterisk (*) indicates an unspecific cross-reaction band observed throughout all lanes, which was subtracted from each individual column signal for quantitative analysis. n = 4 WT hearts. **p<0.01, paired Student's t test.

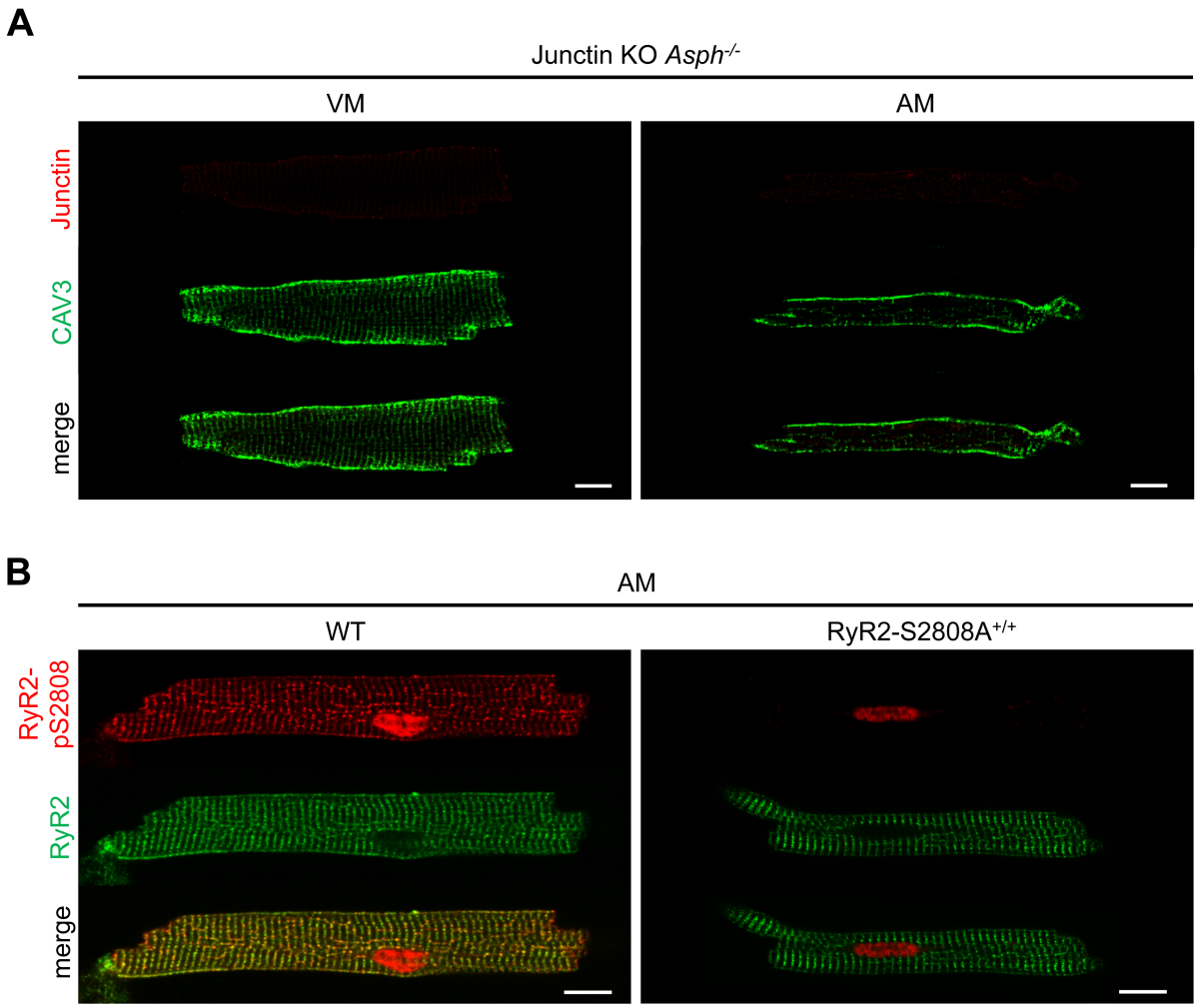

Supplementary Figure 5. Specificity control of the primary junctin and RyR2-pS2808 antibodies in isolated cardiomyocytes. (**A**) Confocal coimmunostaining of junctin and caveolin-3 (CAV3) in isolated ventricular (VM) and atrial myocytes (AM) from junctin knockout (KO) *Asph*$^{-/-}$ mice. Images were acquired and processed using the identical experimental conditions and microscopy settings as applied in **Figure 1E** to verify the junctin primary antibody signal specificity. (**B**) Confocal imaging of isolated mouse AMs from wild-type (WT) versus PKA phosphorylation incompetent RyR2-S2808A$^{+/+}$ knockin mice coimmunostained for the phosphorylated RyR2-Ser2808 epitope (RyR2-pS2808) and RyR2. Whereas the complete absence of the RyR2-pS2808 cluster signals in RyR2-S2808A$^{+/+}$ knockin AMs confirmed the specific cytosolic WT signals, the intranuclear cross-reactivity represents unspecific signals reported previously.[1] Scale bars 10 µm.

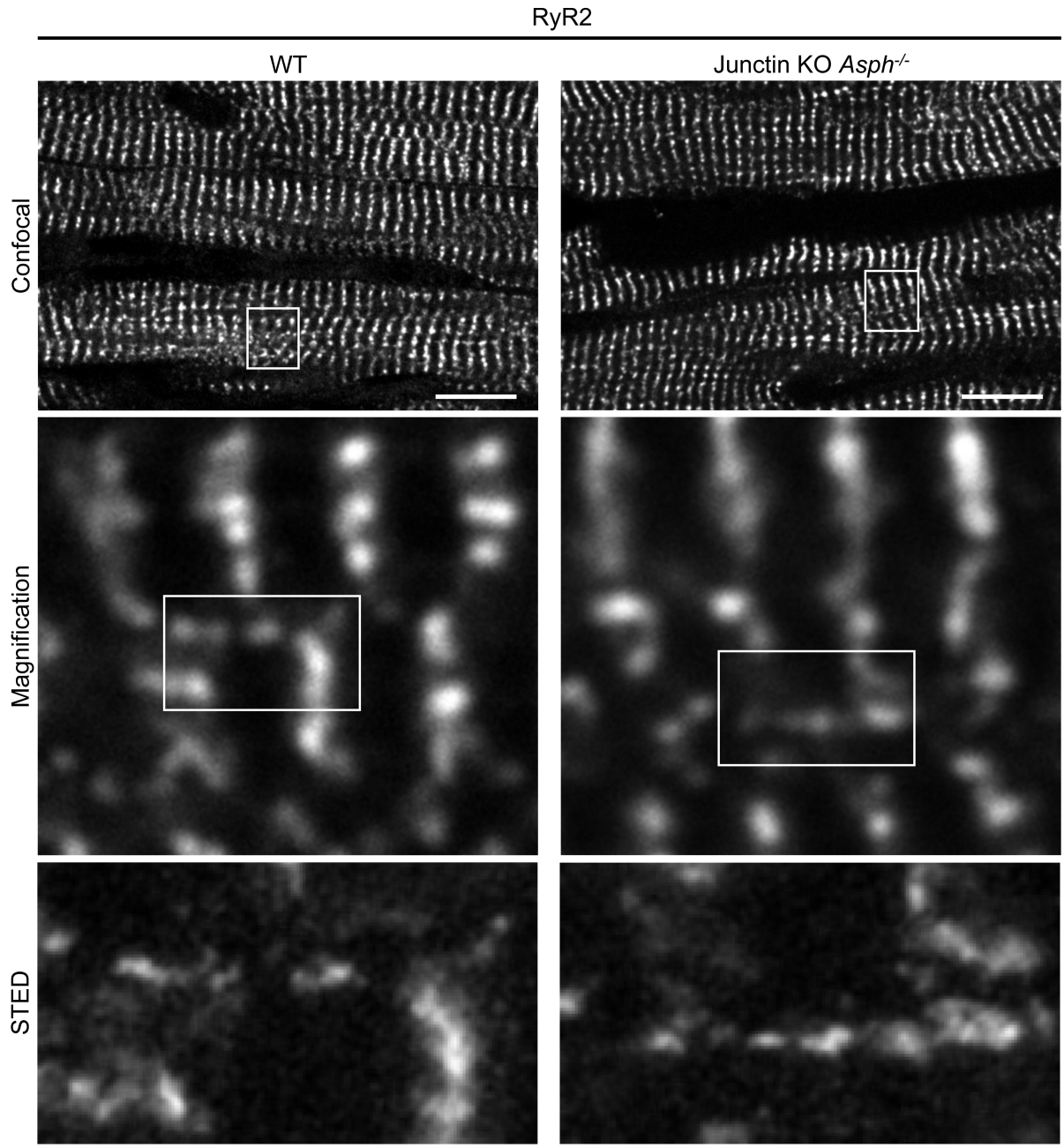

Supplementary Figure 6. Preserved RyR2 clustering in *Asph*$^{-/-}$ atrial myocytes. *Top and middle:* Confocal immunofluorescence imaging of RyR2 in atrial tissue sections from wild-type (WT) and junctin knockout (KO) *Asph*$^{-/-}$ hearts. *Middle*: Magnification of three representative Z-line associated sarcomeric signals showing a preserved transversal distribution of the RyR2 cluster signals. *Bottom*: STED superresolution images documenting a preserved axially aligned RyR2 cluster signal distribution. White boxes indicate sequentially magnified regions. Scale bars 10 µm.

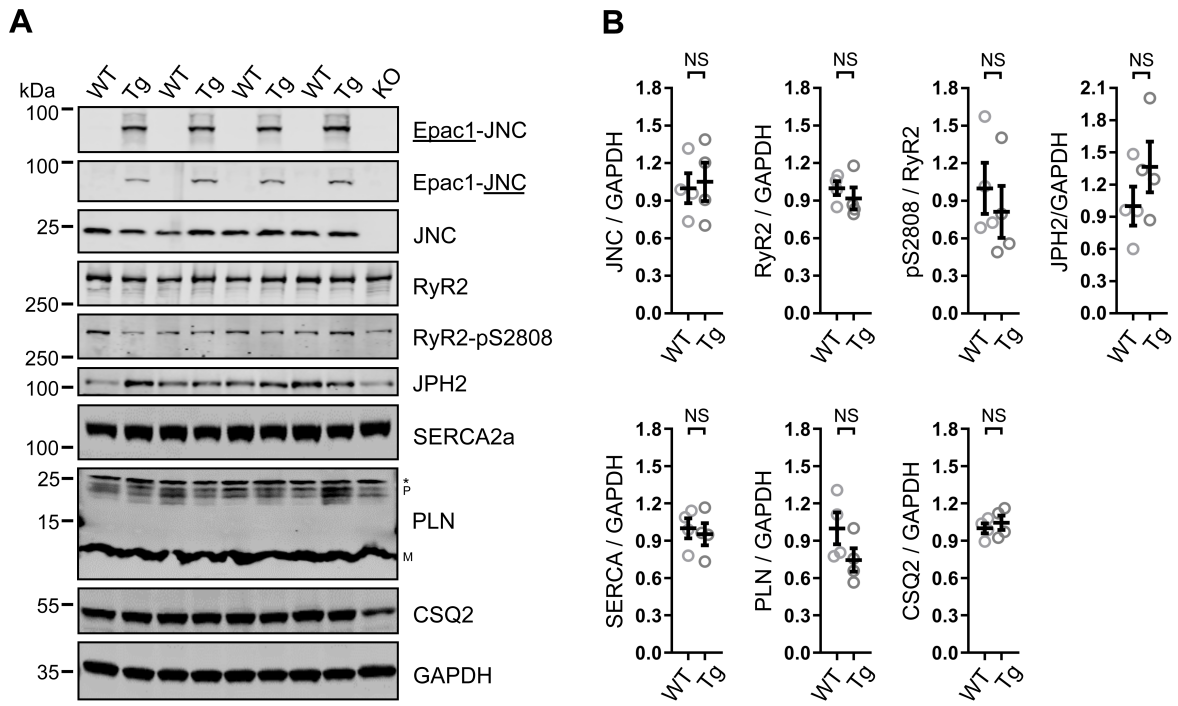

Supplementary Figure 7. Preserved expression of Ca^{2+} handling proteins in Epac1-JNC transgenic atria. (**A**) Immunoblotting of atrial tissue lysates from individual wild-type (WT) versus Epac1-JNC transgenic (Tg) mice, as well as from one control junctin knockout (KO) *Apsh*$^{-/-}$ mouse. Whereas the Epac1-JNC transgenic fusion protein was consistently detected both by antibodies against YFP (Epac1-JNC) and JNC (Epac1-JNC), the specificity of the endogenous junctin bands < 25 kDa was confirmed in the KO atrial tissue lysate. In addition, the following proteins were immunoblotted: JNC, junctin; RyR2, ryanodine receptor type 2; RyR2-pS2808, PKA-phosphorylated RyR2-Ser2808; JPH2, junctophilin-2; SERCA2a, sarcoendoplasmic reticulum Ca^{2+}-ATPase 2a; PLN, phospholamban; P, pentamer; M, monomer; CSQ2, calsequestrin-2; GAPDH, glyceraldehyde 3-phosphate dehydrogenase. Asterisk (*) indicates an unspecific PLN band as revealed by PLN knockout mouse heart lysates (data not shown). (**B**) Dot plots summarizing the indicated protein levels normalized to GAPDH and the substrate-normalized pS2808/RyR2 ratio. PLN was quantified as the sum each of the monomeric and pentameric band signals. $n = 4$ WT and Epac1-JNC transgenic atria each. NS, not significant; unpaired Student's *t* test.

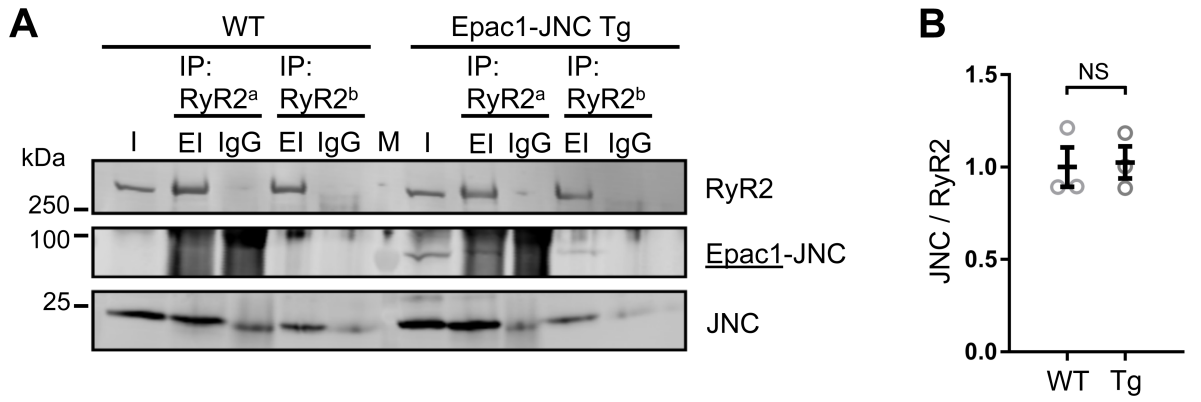

Supplementary Figure 8. Coimmunoprecipitation of transgenic Epac1-JNC and endogenous JNC by RyR2 in atrial tissue lysates. (**A**) Representative coimmunoprecipitation experiment using pooled atrial tissue lysates from each three wild-type (WT) and Epac1-JNC transgenic (Tg) mouse hearts. To exclude any significant interference from unspecific background signals, two distinct antibodies raised in different species were used for RyR2 immunoprecipitation: $RyR2^a$ = rabbit anti-RyR2; $RyR2^b$ = mouse anti-RyR2. Immunoblotting confirmed each the putative and the previously etablished[2] protein-protein interactions of RyR2 with the transgenic Epac1-JNC and the endogenous junctin (JNC), respectively. I, input; El, elution; IgG, negative control; M, molecular weight marker. (**B**) Dot plot comparing the coimmunoprecipitated endogenous JNC to RyR2 ratio in pooled WT versus Epac1-JNC Tg atrial tissue lysates. The data are representative of three individual coimmunoprecipitation experiments as shown in **A**. NS, not significant; unpaired Student's *t* test.

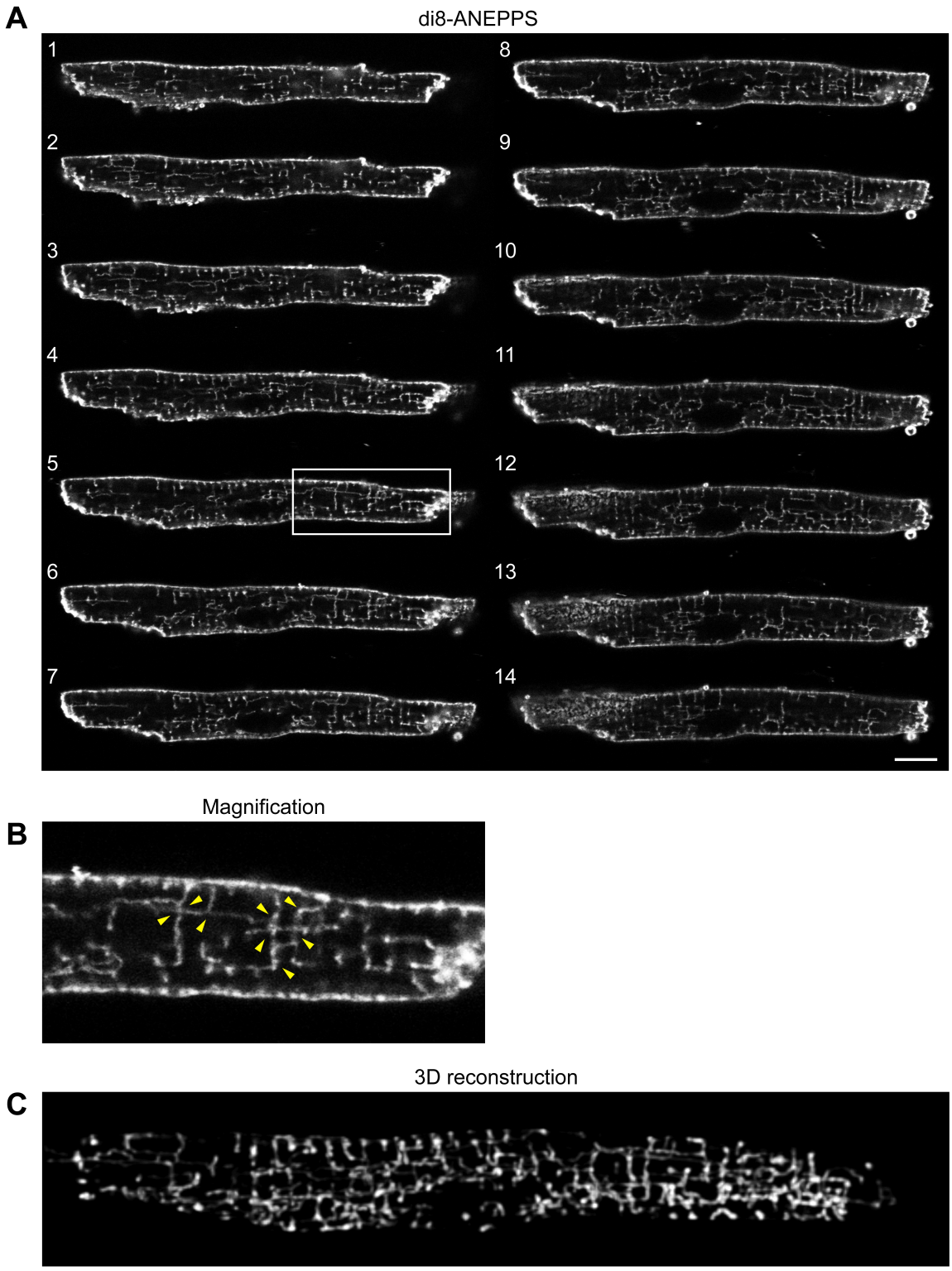

Supplementary Figure 9. Confocal imaging and 3D reconstruction of the TAT network throughout a living atrial myocyte volume confirming abundant axial tubules connected to the surface membrane through transverse tubule components. (**A**) Fourteen consecutive Z-stack images demonstrating the confocal live-cell mapping of the continuous intracellular TAT membrane network stained with the extracellular leaflet marker di-8-ANEPPS (40 µM). Step size 376 nm; scale bar 10 µm. The white box indicates the magnified region in (**B**) highlighting multiple axial-transverse tubule component intersections (yellow arrowheads). (**C**) 3D reconstruction-based intracellular signal Z-stack projection from **A**.

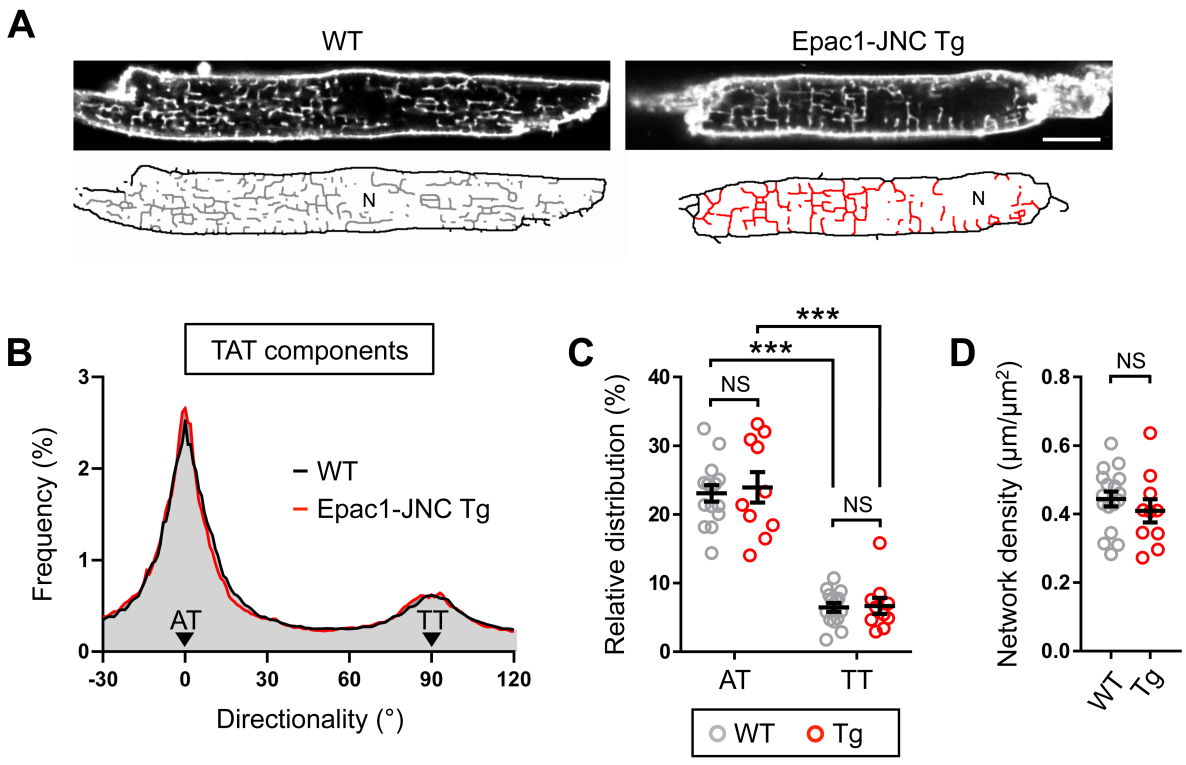

Supplementary Figure 10. Confirmation of preserved TAT network components in Epac1-JCN transgenic atrial myocytes. (**A**) *Top*: Confocal image section of Chol-PEG-KK114 stained intracellular TAT structures in living wild-type (WT) and Epac1-JNC transgenic (Tg) AMs. Scale bar 10 µm. *Bottom*: Binarized continuous membrane signals color-coded for the peripheral surface membrane (*black*) versus the TAT network skeleton (*gray* versus *red*) based on previously published workflows.[3] (**B**) Frequency histograms confirming a preserved, characteristic bimodal distribution of the AM-specific TAT network components. Whereas the major peak confirmed predominant axial tubules (AT) at 0°, the minor peak confirmed sparse transverse tubules (TT) at 90°. (**C**) Dot plot comparing the relative distributions of AT versus TT components in isolated wild-type and Epac1-JCN transgenic AMs. Binning ± 5°. (**D**) Preserved TAT network density in Epac1-JCN transgenic AMs analyzed based on the binarized intracellular skeletons. n = 15 WT / 10 Tg AMs from 3 / 4 mouse hearts in **B-C**, and n = 17 WT / 10 Tg AMs from 3 / 4 mouse hearts in **D**. NS, not significant; ***p<0.001, Student's t test. Of note, the same Epac1-JCN transgenic AMs used here were included for live-cell FRET imaging in **Figure 4A-C**.

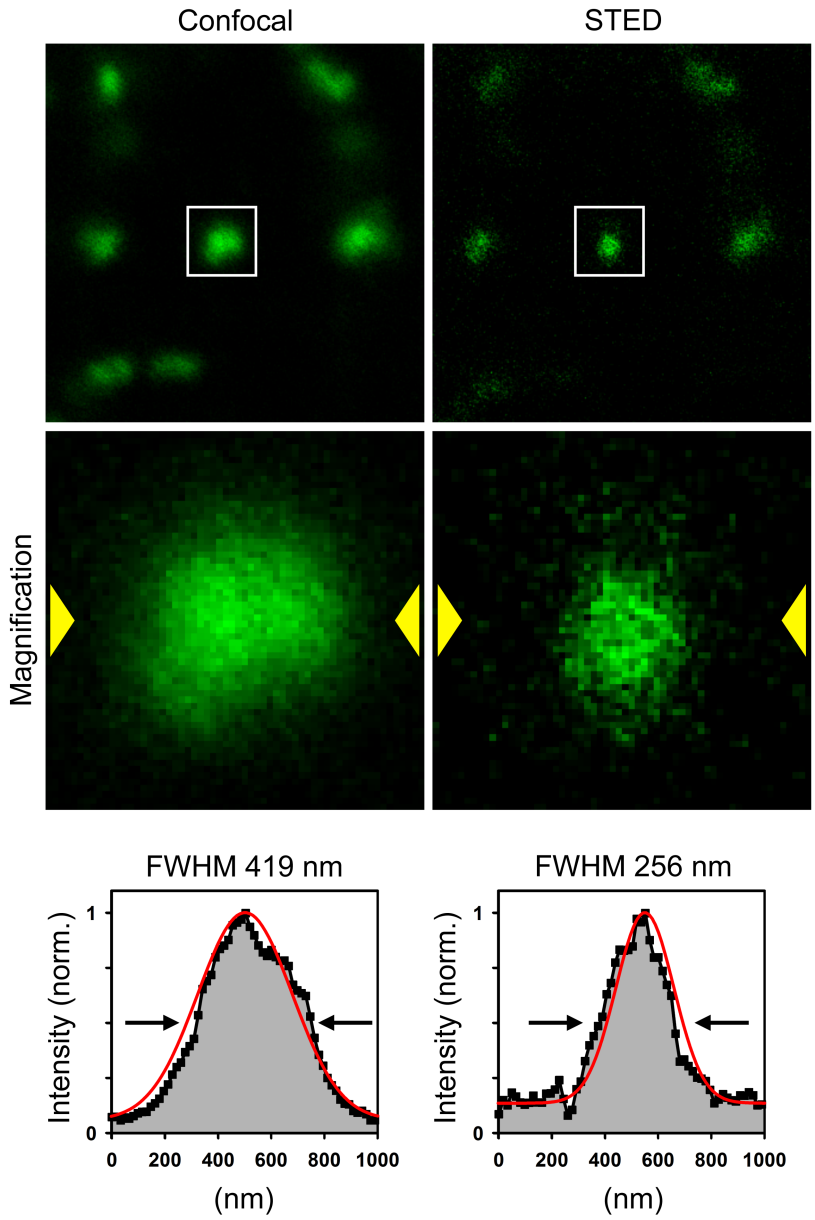

Supplementary Figure 11. Confocal and STED imaging resolution of individual Epac1-JNC clusters in living atrial myocytes. *Top and middle:* Exemplary intracellular confocal and STED image magnifications showing Epac1-JNC clusters excited via the YFP of the FRET biosensor at 514 nm. White boxes indicate magnified regions. Switching ON the STED laser beam at 592 nm apparently increased the lateral signal resolution during live-cell imaging. Yellow triangles indicate the position of the intensity line plots used for further analysis. *Bottom*: Intensity traces (*black*) of the identical Epac1-JNC cluster data comparing the confocal versus STED image from the same living AM. A Gaussian fit (*red*) analyzed the FWHM indicated by the horizontal arrows: confocal 419 nm; STED 256 nm.

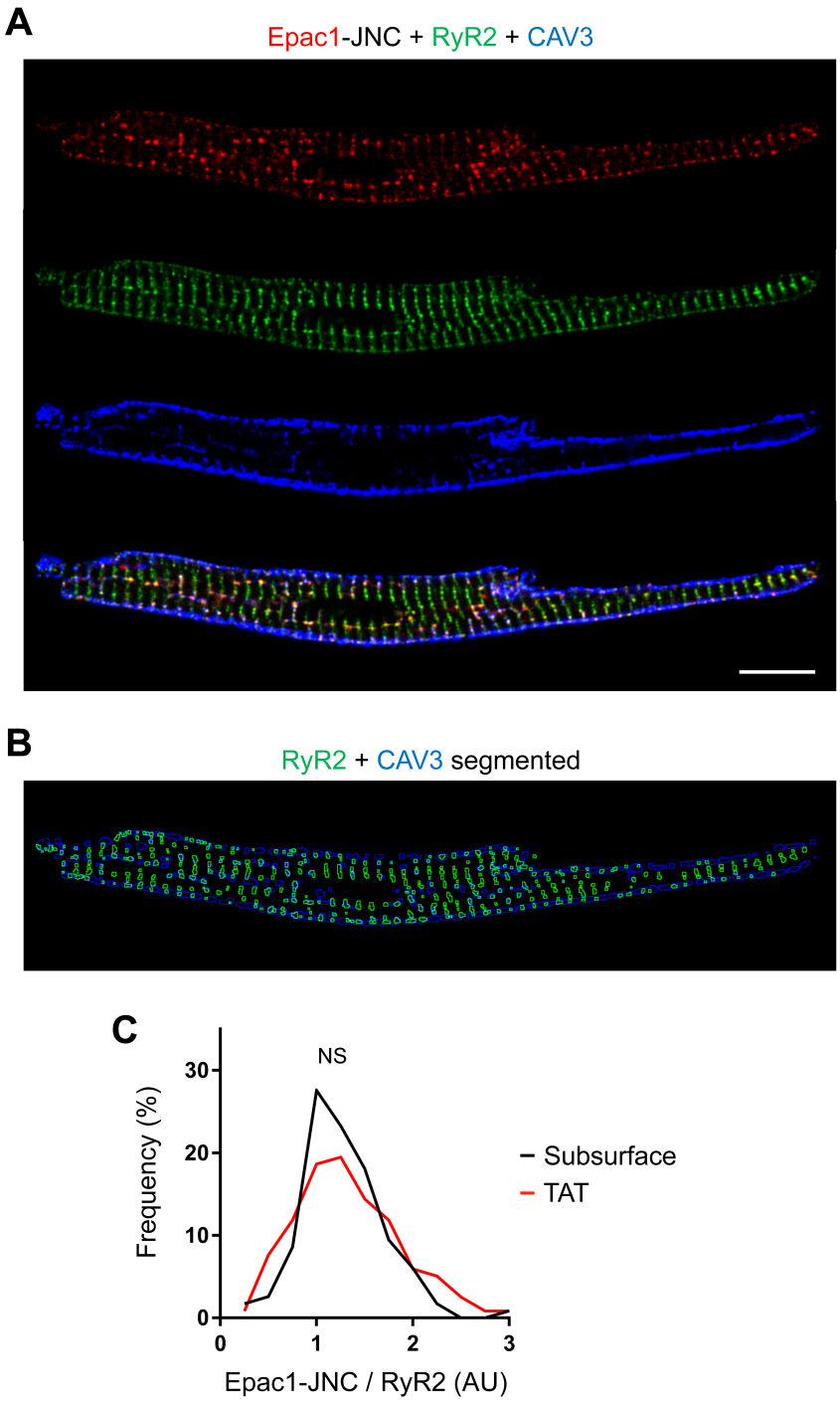

Supplementary Figure 12. Subsurface versus TAT-associated RyR2 clusters show similar Epac1-JNC/RyR2 signal ratios. (**A**) Confocal imaging of an isolated Epac1-JNC transgenic AM triple-immunostained for Epac1-JNC, RyR2 and caveolin-3 (CAV3). Immunostaining images are representative of at least three cell isolations from individual mouse hearts. Scale bar 10 µm. (**B**) RyR2 and CAV3 channel segmentations were generated to analyze the local Epac1-JNC/RyR2 signals at subsurface versus TAT-associated RyR2 clusters. For detailed information please see the **Supplementary Methods** below. (**C**) Histogram of the normalized Epac1-JNC/RyR2 signal distribution confirming a comparable Epac1-JNC expression at subsurface (*black trace*) versus TAT-associated RyR2 clusters (*red trace*). n = 270 subsurface versus 333 TAT-associated RyR2 clusters from 3 AMs. NS, not significant; Mann-Whitney U test.

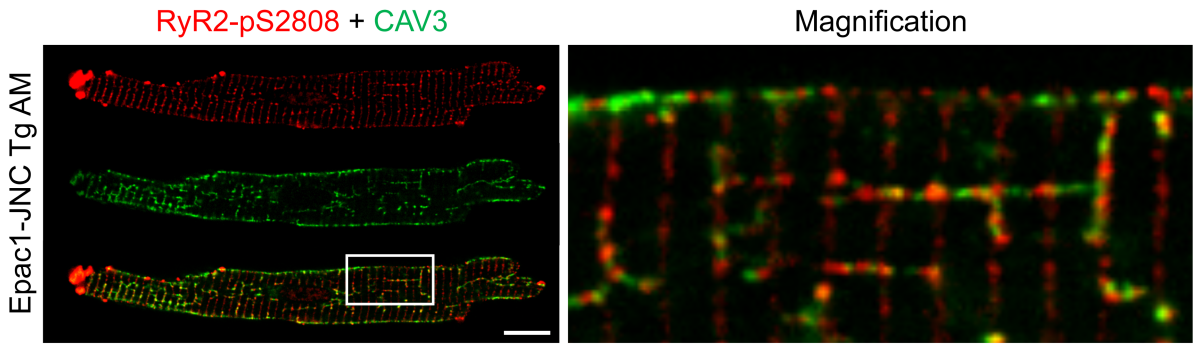

Supplementary Figure 13. Phospho-epitope specific immunofluorescence imaging confirming highly phosphorylated junctional RyR2 clusters in an Epac1-JNC transgenic atrial myocyte. Confocal images showing the coimmunostaining signals of PKA-phosphorylated RyR2-Ser2808 (RyR2-pS2808) clusters at baseline and caveolin-3 (CAV3) clusters, confirming highly phosphorylated junctional versus less phosphorylated non-junctional RyR2 clusters in an isolated Epac1-JNC transgenic (Tg) atrial myocyte (AM). White box indicates the magnified region. Scale bar 10 μm.

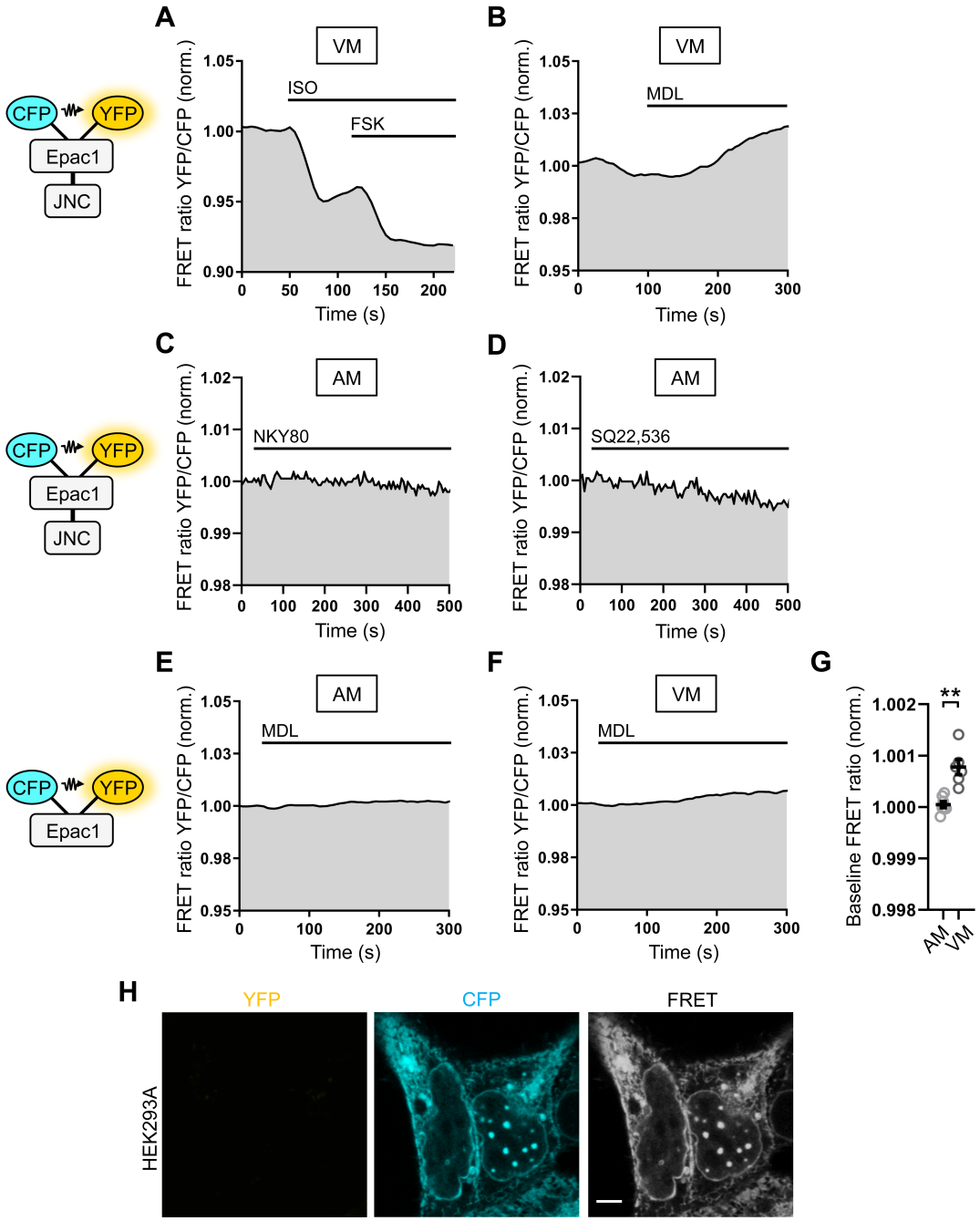

Supplementary Figure 14. Epifluorescence cAMP FRET imaging and correction of CFP bleedthrough for confocal FRET imaging. (**A**) Ventricular myocytes expressing the Epac1-JNC biosensor (*cartoon*) showed robust responses to 100 nM of the β-adrenergic agonist isoproterenol (ISO) and 10 µM of the adenylyl cyclase agonist forskolin (FSK), but (**B**) a moderate response to 100 µM of the adenylyl cyclase inhibitor MDL-12,330A (MDL). (**C-D**) Representative traces showing the epifluorescence FRET signal of transgenic Epac1-JNC atrial myocytes (*cartoon*) treated either with 300 µM NKY80 (**C**) or 100 µM SQ22,536 (**D**). (**E-F**) Representative epifluorescence traces of (**E**) an atrial versus (**F**) a ventricular myocyte transgenically expressing the soluble, cytosolic Epac1-camps biosensor (*cartoon*), each acutely treated with 10 µM MDL-12,330A (MDL). (**G**) Dot plot comparing the basal FRET ratio YFP/CFP in transgenic cytosolic Epac1-camps atrial and ventricular myocytes. $n = 6$ AMs and 7 VMs from 2 mouse hearts. **p<0.001, Student's *t* test. (**H**) Confocal imaging of HEK293A cells overexpressing CFP to determine the amount of spectral bleedthrough into the YFP-FRET channel (emission 405 nm, excitation 550-600 nm) for subsequent correction of the calculated FRET ratio. The bleedthrough correction factor was determined from the average image intensity in the YFP-FRET channel. $n = 10$ cells. Scale 5 µm.

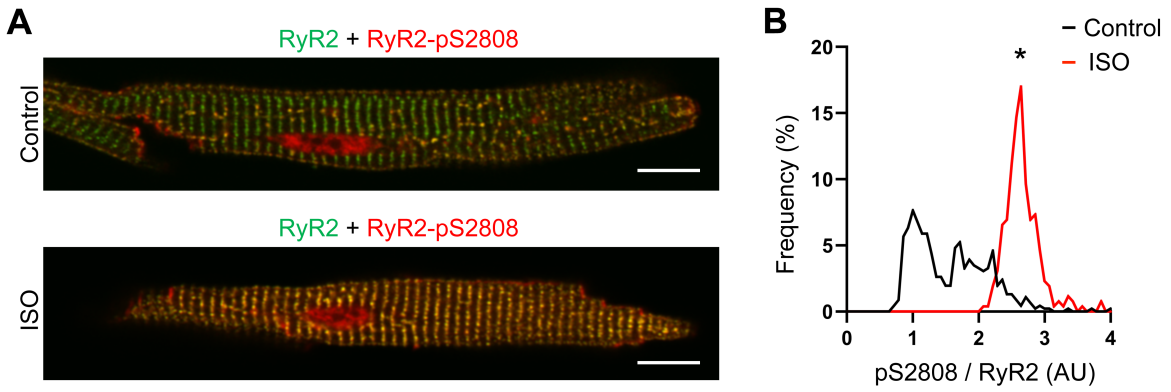

Supplementary Figure 15. Inducible PKA-mediated RyR2 phosphorylation at Ser2808 upon β-adrenergic stimulation. (**A**) Confocal imaging of isolated atrial myocytes coimmunostained for RyR2 and PKA-phosphorylated RyR2-Ser2808 (RyR2-pS2808) either under untreated control conditions or after acute incubation with the β-adrenergic agonist isoproterenol (ISO, 100 nM, 2 min). Under control conditions, intracellular RyR2 clusters along axially oriented string-of-pearl arrangements appeared highly PKA-phosphorylated (*yellow*) in contrast to less or not phosphorylated RyR2 clusters in transverse striation signals (*green*). Following ISO stimulation, RyR2 cluster phosphorylation was strongly and globally increased (*yellow*). Scale bars 10 µm. (**B**) Histogram of the substrate-normalized pS2808/RyR2 cluster signals in untreated control (*black trace*) versus acutely ISO-stimulated (*red trace*) atrial myocytes, confirming the global increase in RyR2-Ser2808 phosphorylation. Histogram data correspond to the exemplary images in **A**. Immunostaining images are representative of at least three cell isolations from individual mouse hearts; control 458 RyR2 clusters, ISO 259 RyR2 clusters. *p<0.05, Mann-Whitney *U* test.

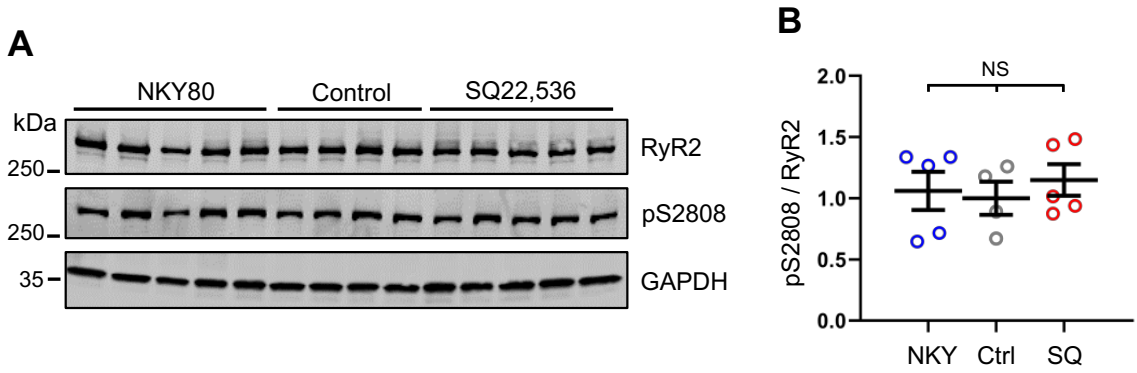

Supplementary Figure 16. The adenylyl cyclase inhibitors NKY80 and SQ22,536 do not significantly affect the pS2808/RyR2 phosphorylation ratio. (**A**) Immunoblotting of RyR2, RyR2-pS2808, and GAPDH comparing atrial tissue lysates from WT mouse hearts perfused with either NKY80 (50 μM, 30 min) or SQ22,536 (100 μM, 30 min) versus untreated control. (**B**) Dot plot summarizing the substrate-normalized pS2808/RyR2 ratio. No significant phosphorylation changes were evident after NKY80 or SQ22,536 treatment. n = 5 mouse hearts each for NKY80 and SQ22,536, and 4 control mouse hearts as indicated by the data points; immunoblots are representative of three technical replicates. NS, not significant; Student's t test.

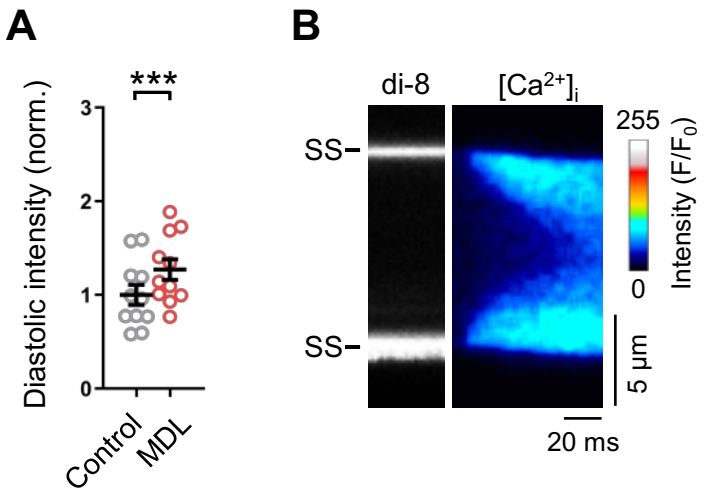

Supplementary Figure 17. Diastolic intracellular Ca^{2+} increase following MDL treatment. (**A**) Dot plot showing the diastolic Fluo-4 signal intensity (F_0) before (control) and 6 min after 10 µM MDL-12,330A (MDL) treatment during 1 Hz field pacing in isolated atrial myocytes. *n* = 11 AMs from 3 mouse hearts. ***p<0.001, Student's *t* test. (**B**) Confocal live imaging showing the localization of the sarcolemmal surface membrane (di-8-ANEPPS, di-8, 40 µM) combined with a 1 Hz field pacing-evoked intracellular Ca^{2+} transient (Fluo-4 AM, 10 µM) in a rare exemplary mouse AM. Transverse line scanning confirmed the apparent U-shaped Ca^{2+} transient configuration throughout the intracellular AM region devoid of TAT membrane structures. Here, the Ca^{2+} signal latency amounted to > 50 ms in the cell center. SS, subsurface sites.

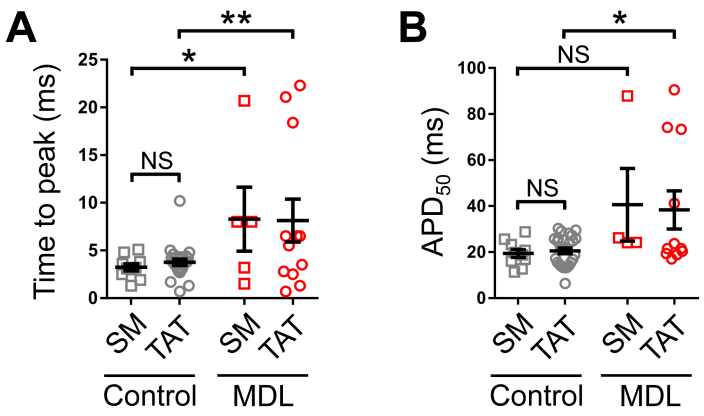

Supplementary Figure 18. Adenylyl cyclase inhibition delays action potential time-to-peak and duration. Dot plots summarizing the indicated action potential parameters in living isolated mouse AMs stained with the voltage-sensitive dye di-4-ANE(F)PTEA (2 µM) for 2-photon recording at baseline and after acute incubation with MDL (10 µM, 3 min). After MDL incubation, (**A**) the time-to-peak was increased both at surface membrane (SM) and transverse-axial tubule (TAT) sites, and (**B**) the action potential duration at 50% repolarization (APD_{50}) was significantly increased at transverse-axial tubule (TAT) sites. However, no difference was observed between the SM versus TAT locations either under control conditions or after MDL treatment. *n* = 10 surface versus 26 TAT measurements in 10 cells under control conditions, and 5 (**A**) / 4 (**B**) surface versus 12 (**A**) / 11 (**B**) TAT measurements in 5 cells following MDL treatment from 3 mouse hearts. NS, not significant, *p<0.05, **p<0.01, Student's *t* test.

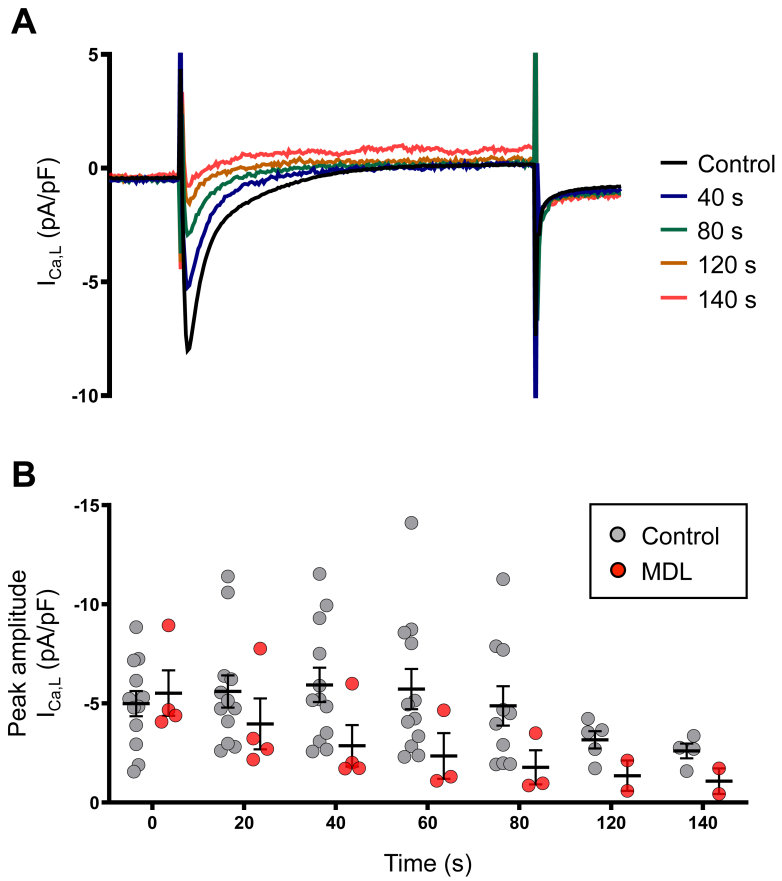

Supplementary Figure 19. Time course of the L-type Ca^{2+} current density after MDL application. (**A**) Superimposed $I_{Ca,L}$ current traces from an exemplary voltage-clamped AM at different time points after MDL application (10 µM). (**B**) Time course of the peak $I_{Ca,L}$ current amplitude in AMs under control versus MDL treatment (10 µM). The inhibitory MDL effect occurs prompt and markedly earlier compared to the spontaneous $I_{Ca,L}$ current run-down. *n* = 12 control versus 2-4 MDL treated AMs from 6 / 2-4 mouse heart isolations.

Perfusion buffer	NaCl 120.4, KCl 14.7, KH_2PO_4 0.6, Na_2HPO_4 0.6, $MgSO_4$ 1.2, HEPES 10, $NaHCO_3$ 4.6, taurine 30, 2,3-butanedione-monoxime 10, glucose 5.5, pH 7.4
Epifluorescence FRET buffer	NaCl, 144, KCl 5.4, $MgCl_2$ 1, $CaCl_2$ 1, HEPES 10, pH 7.4
Tyrode's solution	NaCl 140, KCl 5.4, $MgCl_2$ 1.2, HEPES 10, Na_2HPO_4 0.33, $CaCl_2$ 1.2, glucose 10, pH 7.4
RAMP Tyrode's solution	NaCl 113, KCl 4.7, $MgCl_2$ 1.2, glucose 10, and HEPES 10, pH 7.3-7.35
Patch-clamp bath solution	NaCl 140, HEPES 10, KCL 4, probenecid 2, $MgCl_2$ 1, glucose 10, $CaCl_2$ 0.9, 4-AP 5, $BaCl_2$ 0.1, pH 7.45
Patch-clamp pipette solution	K^+-aspartate 92, KCl 48, Mg-ATP 1, Na_2-ATP 4, EGTA 0.02, GTP-Tris 0.1, HEPES 10, pH 7.2
CoIP buffer	NaCl 150, Tris/HCl 50, EDTA 1, CHAPS 0.15% (w/v), pH 7.4

Supplementary Table 1. Composition of physiological buffer solutions as referenced in the methods section in mM.

Supplementary Table 2. Primary antibodies used in immunofluorescence imaging and Western blotting as referenced in the figure legends or methods section.

Protein of interest	Species	Clonality	Clone	Antigen / Immunogen	Company	Catalog no.	Concentration	Dilution WB	Dilution IF	IF cross reaction
Adenylyl cyclase VI	rabbit	polyclonal		rat adenylyl cyclase VI aa 13-27 conjugated to keyhole limpet haemocyanin	Abcam	ab14781	0.78 mg/ml		1:500	no
Aspartyl/asparaginyl β-hydroxylase	mouse	monoclonal	A-10	human ASPH aa. 382-681	Santa Cruz Biotechnology	sc-271391	200 µg/ml	1:200		
Calsequestrin-2	rabbit	polyclonal		purified canine cardiac calsequestrin	Thermo Fisher Scientific	PA1-913		1:1000		
Caveolin-3	mouse	monoclonal	26/ Caveolin 3	rat caveolin-3 aa. 3-24	BD Biosciences	610421	250 µg/ml		1:500	no
GAPDH	mouse	monoclonal	6C5		Biotrend	5G4 Mab6C5	5.3 mg/ml	1:80.000		
Junctin	rabbit	polyclonal		aa. GHAHVSKENGQKRKN	custom-made			1:500	1:600	no
Junctophilin-2	rabbit	polyclonal		synthetic peptide derived from C-terminal region of mouse junctophilin-2	Thermo Fisher Scientific	40-5300	0.25 mg/ml	1:500		
Phospholamban	mouse	monoclonal	2D12	synthetic peptide corresponding to dog phospholamban aa. 2-25	Abcam	ab2865		1:1000		
Ryanodine receptor 2	mouse	monoclonal	C3-33	canine cardiac RyR	Thermo Fisher Scientific	MA3-916	1 mg/ml		1:500	no
Ryanodine receptor 2	rabbit	polyclonal		aa. QDEVRGDGEEGERKPLEAALPSEDLTDLKELTE ESDLLSDIFGLDLKREGGQYKLIPHNPNAGLSDLMS NPVPMPEVQEKFQEQKAKEEEKEEKEETKSEPE	Sigma-Aldrich	HPA020028	0.18 mg/ml	1:2500		
Ryanodine receptor 2 phosphoSerin2808	rabbit	polyclonal		synthetic peptide (YNRTRRIS(PO_3H_2)QT_{2810}) conjugated to keyhole limpet haemocyanin	Badrilla Ltd.	A010-30		1:1000	1:250	yes (nucleus)
Ryanodine receptor 2 phosphoSerin2814	rabbit	polyclonal		synthetic peptide (TSQVS(PO_3H_2)$VDAAH_{2819}$) conjugated to keyhole limpet haemocyanin	Badrilla Ltd.	A010-31		1:1000		
SERCA2a	rabbit	polyclonal		synthetic peptide (C-LEPAILE997) corresponding to aa. at the extreme C-terminus of SERCA2a	Badrilla Ltd.	A010-20		1:1000		
YFP	rabbit	polyclonal		purified recombinant eGFP	Thermo Fisher Scientific	CAB4211	1 mg/ml	1:1000		

Supplementary Methods

Mouse models

All animal studies were performed in accordance with Directive 2010/63/EU of the European Parliament. If not stated otherwise, we used mice back-crossed into the C57BL/6N background for at least 10 generations, both female and male aged 10-16 weeks. The generation of Epac1-JNC transgenic mice is described in a parallel manuscript,[4] and Epac1-camps transgenic mice were characterized previously.[5] Junctin knockout mice *Asph*$^{-/-}$, generated in the C57BL/6J background as described previously,[6] were used to validate the specificity of the custom-made anti-junctin antibody by immunofluorescence imaging (**Supplementary Figure 5**) and Western blotting (**Figure 1A**). The generation of RyR2-S2808A$^{+/+}$ knockin mice was described previously.[7]

Atrial and ventricular myocyte isolation from mouse hearts

For isolation of AMs and VMs, 10-16 weeks old mice were euthanized by cervical dislocation following isoflurane anesthesia. Hearts were rapidly excised, cannulated with a 21 G cannula and perfused with nominally Ca^{2+} free perfusion buffer (**Supplementary Table 1**) for 4 min at 37°C and a constant flow rate of 4 ml/min. Next, collagenase type II containing perfusion buffer (600 U/ml, Worthington) was used for approximately 10 min. Next, the atria and ventricles were carefully separated using a binocular microscope and triturated with a pipette (1 ml, 86.1251.025, Sarstedt) to isolate myocytes in cell suspension.[3]

Immunofluorescence microscopy

Isolated cardiomyocytes were fixed with 4% PFA on laminin-coated coverslips and permeabilized in blocking buffer (0.2% Triton, 10% bovine calf serum in PBS). Next, cells were incubated overnight at 4°C with the primary antibody at the final dilution in blocking

buffer. Please see **Supplementary Table 2** for detailed information. For generation of a junctin-specific antibody, we used an immunogen based on the C-terminus of junctin, which is not shared by other splice variants of the *Asph* gene.[8] Following three washing steps, secondary antibodies coupled to bright fluorophores were added at a dilution of 1:1000 for 2 h at room temperature: goat anti-rabbit STAR635P (2-0012-007-2, Abberior), goat anti-rabbit STAR580 (ST580, Abberior), goat anti-mouse STAR580 (2-0002-005-1, Abberior) or goat anti-mouse STAR488 (2-0002-006-8, Abberior). The Epac1-JNC transgene was detected by a single-domain antibody directly coupled to Abberior Star635P (FluoTag X4-anti-GFP conjugated to STAR635P, dilution 1:500, N0304-Ab635P-S, NanoTag Biotechnologies) (**Figure 2F** and **G**, **Supplementary Figure 1C**). Coimmunostaining by combined mouse antibodies (**Figure 1F**) required direct labelling of one primary antibody with Zenon Alexa Fluor 555 mouse IgG labelling reagent as per the manufacturer's instruction (Z25008, Thermo Fischer Scientific). Subsequently, samples were washed three times with PBS and mounted on glass coverslips in mounting medium (ProLong Gold antifade reagent, Thermo Fischer Scientific).

Confocal 8-bit images were acquired with a Leica TCS SP8 microscope and a 100x/1.40 oil objective (HC PL APO C2S, Leica). A pixel size of 0.11 µm x 0.11 µm, 16x line averaging, 600 Hz scanning speed and a pixel dwell time of 400 ns were applied. For secondary antibody excitation and detection the following settings were applied: STAR635P was excited at 635 nm and emission detected between 650-700 nm; STAR580 was excited at 580 nm and emission detected between 600-630 nm; and STAR488 was excited at 488 nm and emission detected between 515-560 nm. STED immunofluorescence images were acquired using a pixel size of 16.23 x 16.23 nm with 32x line averaging, 600 Hz scanning speed, a pixel dwell time of 400 ns, and a 775 nm depletion laser beam for the fluorophores STAR635P and STAR580. Confocal and STED immunofluorescence images were acquired with an effective PSF of 289 ± 5 nm and

70.2 ± 6.4 nm, respectively, as determined by FWHM measurements of 40 nm beads excited at 640 nm (AS-595-775-NP, Abberior), shown in **Supplementary Figure 1**.

For image segmentation in **Figure 1B-C** and **E**, raw images were subjected to local background subtraction (rolling ball radius: 20 pixels), Gaussian blurring (sigma: 1) and segmented by local Bernsen thresholding (radius: 15 pixels) using ImageJ/Fiji (https://imagej.net/Fiji). Any percentage of signal overlap between the two channels was defined as overlapping clusters.

In situ pS2808/RyR2 cluster analysis was performed as described previously.[1] Unspecific intranuclear RyR2-pS2808 signals were excluded from analysis.

To analyze the Epac1-JNC/RyR2 immunofluorescence signal ratio of subsurface versus TAT-associated junctional RyR2 clusters in **Supplementary Figure 12**, RyR2 and CAV3 channels were subjected to local background subtraction (rolling ball radius: 25 pixels), Gaussian blurring (sigma: 1) and segmented by local Bernsen thresholding (radius: 15 pixels). The segmented RyR2 channels were used to create global RyR2 cluster ROIsets, which were manually subdivided into subsurface versus intracellular RyR2 clusters. Subsurface ROIs (subsurface RyR2 clusters) and intracellular ROIs overlapping with segmented CAV3 signals (TAT-associated RyR2 clusters) were used to calculate the Epac1-JNC/RyR2 immunofluorescence ratio within each ROI based on the raw Epac1-JNC and RyR2 signals.

Histological immunostaining in atrial mouse tissue as shown in **Supplementary Figure 6** was performed as described previously.[9]

***Fourier* transformation analysis of RyR2 and junctin signals**

Equally sized intracellular ROIs (20.45 µm x 5.68 µm) of dual-color immunofluorescence stainings for RyR2 and junctin in isolated cardiomyocytes were rotated to align the cellular transverse striation with the vertical axis of the image. Fast *Fourier* transformation in ImageJ/Fiji was performed and the power of periodic frequencies compared for both RyR2 and junctin in VMs and AMs.

Live-cell STED imaging

For superresolution imaging of TAT membrane structures and the Epac1-JNC biosensor (**Figure 2E** and **Supplementary Figure 11**), isolated Epac1-JNC AMs were incubated with 1 µM Chol-PEG-KK114 (custom synthesis)[10] in perfusion buffer (**Supplementary Table 1)** for 10 min on laminin-coated glass-bottom imaging chambers and subsequently washed three times. For image acquisition, we used a Leica TCS SP8 STED system with a HC PL APO C2S 100x/1.40 oil objective and a pixel size of 16.23 x 16.23 nm with 32x line averaging, 600 Hz scanning speed and a pixel dwell time of 400 ns. Chol-PEG-KK114 was excited at 635 nm with STED depletion at 775 nm and fluorescent emission detected between 650-700 nm. The Epac1-JNC biosensor was located via YFP detection with excitation at 514 nm and emission detection between 523-600 nm without STED depletion as shown in **Figure 2E**. Additionally, STED depletion at 592 nm was applied to increase resolution as shown in **Supplementary Figure 11**.

Epifluorescence FRET measurements

Isolated AMs and VMs from Epac1-JNC or Epac1-camps mice were allowed to settle over laminin-coated glass coverslips. Adhered cells were transferred to imaging medium (**Supplementary Table 1**) and treated with isoproterenol, forskolin, MDL-12,330A, NKY80 or SQ22,536 (all from Sigma-Aldrich) as indicated. The percentage of FRET change (YFP/CFP) was measured in an inverted Leica microscope (DMI3000b) fitted with a 63x oil

objective, coolLED (440 nm) for excitation, Dualview beam splitter (Photometrics) for CFP and YFP emission filters, and a Qimaging camera. The FRET ratio was corrected for donor bleedthrough.

Confocal FRET measurements

Imaging

For confocal FRET experiments, isolated Epac1-JNC AMs were incubated with 1 µM Chol-PEG-KK114 in perfusion buffer (**Supplementary Table 1)** for 10 min on laminin-coated glass-bottom imaging chambers and subsequently washed three times. Confocal images were acquired with a Zeiss LSM 880 microscope using a Plan-Apochromat 63x/1.40 oil objective with a pixel size of 100 x 100 nm. For FRET measurements, four channels were acquired:

1) YFP (excitation 514 nm, emission detection 550-600 nm)

2) CFP (excitation 405 nm, emission detection 450-500 nm)

3) YFP-FRET (excitation 405 nm, emission detection 550-600 nm)

4) Chol-PEG-KK114 (excitation 633 nm, emission 650-700 nm)

All channels were acquired with 16x line averaging and a pixel dwell time of 400 ns. We used the Zeiss ZEN firmware to reliably reproduce laser settings. Laser intensity settings were defined by a) the laser output values (laser power ex objective 405 nm 6.18 mW; 514 nm 1.37 mW; 633 nm 1.5 mW) and b) Acousto-Optic Tunable Filter (AOTF) attenuation settings expressed in per cent (2%). Confocal FRET images were acquired with an effective PSF of 330.0 nm ± 5.9 nm as determined by FWHM measurements of 40 nm beads (**Supplementary Figure 1**). FRET experiments were performed in fresh perfusion buffer (**Supplementary Table 1)** at room temperature. Cell inclusion was based on the following criteria independently of

experimental grouping: intact cell surface boundary, regular sarcomeric striations, TAT network integrity, and sufficient Epac1-JNC sensor expression as judged by YFP signal intensity. For pharmacological protocols, cells were treated with 100 nM isoproterenol (I6504, Sigma-Aldrich) or 100 µM MDL-12,330A (M182, Sigma-Aldrich) diluted with DMSO in perfusion buffer.

Analysis

To perform localized subcellular FRET analysis, we firstly used the following algorithm to create a global ROIset of all subcellular Epac1-JNC biosensor clusters: confocal images of channel 1) (YFP; excitation 514 nm, emission 550-600 nm), were subjected to local background subtraction (rolling ball radius: 20 pixels), Gaussian blurring (sigma: 1) and segmented by local Bernsen thresholding (radius: 15 pixels). To differentiate between subsurface- and TAT-associated biosensor locations, we secondly segmented images of channel 4) (Chol-PEG-KK114; excitation 633 nm, emission 650-700 nm) by smoothing, local background subtraction (rolling ball radius: 5 pixels), local contrast enhancement (radius: 49 pixels, slope: 3) and local Bernsen thresholding (radius: 25 pixels). Next, the membrane segmentation was split between surface sarcolemma and intracellular TAT signals by a manually created ROI. Subsequently, the global biosensor ROIset from channel 1) was overlaid with both separate membrane segmentations from channel 4) to define subsurface- or TAT-associated Epac1-JNC biosensor clusters. Non-overlapping clusters were disregarded. Intensities in channel 2) (CFP; excitation 405 nm, emission 450-500 nm) and channel 3) (YFP-FRET; excitation 405 nm, emission 550-600 nm) were then measured within subsurface- and TAT-associated ROIsets and exported into Excel. FRET ratios were determined as YFP/CFP where every ROI represented one individual cluster. Finally, individual cluster-based FRET ratios of both groups were averaged to cellular means. The analysis strategy was visualized in **Figure 3E-I** for further explanations.

The corresponding YFP/CFP FRET ratios were corrected for systematic linear CFP bleedthrough in the YFP-FRET channel determined by CFP plasmid transfection in HEK239A cells (**Supplementary Figure 14H**) as previously described for epifluorescence FRET imaging.[11]

Combined axial tubule and Ca^{2+} imaging

Freshly isolated AMs were plated on laminin-coated glass-bottom imaging chambers (custom made) and gradually reintroduced to increasing Ca^{2+} concentrations in Tyrode's solution (**Supplementary Table 1**). Cells were incubated in 1 µM Chol-PEG-KK114 or 40 µM di-8-ANEPPS (D3167, Thermo Fisher Scientific) for 10 min, and 10 µM Fluo-4 AM (F14201, Thermo Fisher Scientific) for 25 min. After washing with fresh Tyrode's solution, imaging was performed on a Zeiss LSM 880 microscope using a Plan-Apochromat 63x/1.40 oil objective. Chol-PEG-KK114 was excited at 633 nm and detected between 650-700 nm, di-8-ANEPPS was excited at 458 nm and detected between 550-740 nm, and Fluo-4 was excited at 488 nm and detected between 493-622 nm. Ca^{2+} transients were recorded at room temperature during 1 Hz electrical field stimulation with 3 ms voltage steps at 23 V. For recordings in steady-state stimulation, myocytes were paced for five times prior to imaging. Ca^{2+} transients were recorded in transverse line scanning at 0.1 µm pixel size and a scanning speed of 0.806 ms per line. After recording under control conditions, cells were incubated for 6 min in 10 µM MDL-12,330A for measurements under treatment conditions. For subcellular Ca^{2+} transient analysis, the maxima of the Chol-PEG-KK114 or di-8-ANEPPS line profile were used to define surface sarcolemma and axial tubule locations. Ca^{2+} signals within a 1 µm radius of the Chol-PEG-KK114 or di-8-ANEPPS maxima were considered as surface sarcolemma or axial tubule-originated local Ca^{2+} signals. Local early Ca^{2+} release latencies were determined as Fluo-4 signal rise above 25% of baseline intensity for each axial tubule, subsurface and cytosolic locations in reference to Chol-PEG-KK114 or di-8-ANEPPS membrane signals.

SR Ca^{2+} load measurements

For SR Ca^{2+} load experiments, AMs isolated from WT mice were gradually reintroduced to increasing Ca^{2+} concentrations in Tyrode's solution and subsequently incubated with 10 µM Fluo-4 AM (F14201, Thermo Fisher Scientific) on laminin-coated glass-bottom imaging chambers as described above. Imaging was performed on a Zeiss Axio Observer A1 microscope equipped with a PlanApochromat 40x/1.4 oil immersion objective, a Polychrome V light source and a CoolSNAP-HQ2 CCD-camera (Visitron Systems, Pullheim, Germany) at room temperature. SR Ca^{2+} load was determined as the peak of the Ca^{2+} transient induced by adding 10 mM caffeine after normalizing signals to baseline fluorescence. Tau decay was analyzed by fitting the decay of caffeine induced transients. AMs from the same hearts were measured under control conditions or 6 min after MDL-12,330A (10µM) treatment before and after adding caffeine.

Random access multi-photon (RAMP) recordings

For RAMP recordings, cells were resuspended in Tyrode's solution (**Supplementary Table 1**). Isolated AMs were stained for 15 min with 2 µg/ml of di-4-AN(F)EPPTEA,[12] and then resuspended in fresh Tyrode's solution containing blebbistatin and cytochalasin D. The measurement was performed on the same cell before and after MDL incubation (10 µM for 3 min). Staining and imaging sessions were performed at room temperature (20-22°C). The imaging was performed during steady-state stimulation (0.34 Hz). The RAMP microscope has been described previously.[13, 14] Briefly, the excitation light is provided by a 1064 nm fibre laser and it is focused onto the specimen by the objective lens (40 × 1.0 NA) passing through a scanning head provided by orthogonally oriented acousto-optic deflectors (AODs). An oil immersion condenser (1.4 NA) and the objective collect the two-photon fluorescence signal in forward and backward, respectively. The detection of fluorescence signals is performed by two photomultiplier tubes (H7422, Hamamatsu) using an emission filter of 655 ± 20 nm. In order

to reach action potential threshold, square pulses of 10–20 V and duration of 3 ms were used placing cells in a field-stimulated chamber with two parallel platinum wires (250 µm in diameter) placed at a distance of 6.3 mm. In a typical measurement, the acousto-optic deflectors rapidly scan lines on different membrane segments (4-5) with an integration time on each line of about 0.1 - 0.2 ms, leading to a temporal resolution of the order of 0.5 - 1 ms. The spatial resolution of the RAMP system is in the order of 0.6 µm radially and 1.7 um axially (FWHM).

Voltage-Clamp and combined FRET measurements

Voltage clamp experiments on mouse AMs were performed in whole cell ruptured patch configuration to measure $I_{Ca,L}$.[15] The cells were superfused at 37°C with a bath solution (**Supplementary Table 1**). For the inhibition of K^+ currents, 4-aminopyridine (5 mM) and $BaCl_2$ (0.1 mM) were added to the bath solution. Borosilicate glass microelectrodes had tip resistances of 3-5 MΩ when filled with an electrode solution (**Supplementary Table 1**). Seal resistances were 2-6 MΩ. pClamp-software (V10.7, Molecular Devices, Sunnyvale, CA, United States) was used for data acquisition and analysis. Series resistance and cell capacitance were compensated. A ramp protocol was used with a frequency of 0.5 Hz to activate $I_{Ca,L}$. For this purpose, cells were clamped at a holding potential of -80 mV followed by a ramp pulse depolarization to -40 mV for 500 ms to inactivate the fast Na^+-current ending with a 100 ms square pulse to +10 mV. Peak current amplitude was normalized to cell capacitance, an approximation of cell surface area, to ascertain current density. 10 µM MDL-12,330A was applied with a pressurized flow perfusion system (OctaFlow II, ALA science, Farmingdale, NY, United States), as peak current reached steady state.

Combined FRET and L-type Ca^{2+}-current measurements were accomplished using an inverted fluorescent microscope (Olympus IX71), an UPlanSApo 60x/1.35 Oil (Olympus) objective, a polychrome V light source (Till Photonics), a beam splitter (Mag Biosystems DV2), and a CCD camera (Andor iXON). CFP was excited at 440 nm every 5 s for a total of 250 ms. MetaFluor

software (V7.7, Molecular Devices, Sunnyvale, CA, United States) was used for the imaging data acquisition of CFP and YFP signals. The FRET ratio was calculated in Excel and corrected for donor bleedthrough. FRET imaging was started after steady state in L-type Ca^{2+}-current was reached. $I_{Ca,L}$ recordings were executed as described above. MDL was added after a stable baseline of the FRET ratio had appeared.

Immunoblot protein analysis

For protein analysis, mouse hearts were *Langendorff*-perfused for 2 min with isotonic NaCl solution at 37°C. After dissection under binoculars, atrial and ventricular mouse heart samples were directly frozen in liquid nitrogen and stored at -80°C. Using a Miccra D-1 homogenizer, cardiac tissue was homogenized in ice-cold buffer (in mM: HEPES 10, sucrose 300, NaCl 150, EGTA 1, $CaCl_2$ 2, Triton X-100 0.5% (v/v), protease and phosphatase inhibitor mix (Roche), pH 7.4). The homogenized tissue was solubilized for 30 min at 4°C by rotation and subsequently centrifuged at 8000 × *g* for 10 min at 4°C to obtain the post-nuclear fraction. Pierce BCA protein Assay Kit (Thermo Fisher Scientific) was used to determine protein concentrations. For immunoblotting, 20 µg of protein per lane were resolved by SDS-PAGE using 4-20% Tris-HCl protein gels (3450033, Bio-Rad). Using the Bio-Rad criterion blotter (plate electrodes), proteins were transferred onto PVDF membranes (0.45 µm, Immobilon-FL, Merck Millipore). Membranes were blocked for 1 h in 5% (w/v) non-fat milk in Tris-buffered saline with 0.05% (v/v) Tween 20 and incubated with primary antibodies over night at 4°C. Please see **Supplementary Table 2** for detailed primary antibody information. After washing, blots were incubated with fluorescently labelled anti-rabbit or anti-mouse secondary antibodies at a dilution of 1:10,000 for a minimum period of 1 h at room temperature (donkey anti-mouse P/N 926-68072, donkey anti-mouse P/N 925-32212, donkey anti-rabbit P/N 926-32213, donkey anti-rabbit P/N 926-68073, LI-COR). Membranes were developed with the Odyssey CLx

imaging system (LI-COR), and Image Studio Lite Version 5.2 was used to analyse band densities. All proteins were normalized to GAPDH.

Co-immunoprecipitation of RyR2 and Epac1-JNC in atrial tissue

For co-immunoprecipitation, atrial tissue from WT and Epac1-JNC transgenic mice was harvested as described above. In short, tissue was harvested after *Langendorff*-perfusion with isotonic NaCl solution for 2 min and subsequently lysed in CoIP buffer (**Supplementary Table 1**) using a Miccra D-1 homogenizer. In total, three atria from Epac1-JNC and three WT mice, respectively, were pooled. Cell debris was removed by centrifugation at 8000 × g for 10 min at 4°C. The supernatant was used for protein concentration determination (Pierce BCA protein Assay Kit, Thermo Fisher Scientific). For each co-immunoprecipitation, protein concentration was adjusted to yield 300 µg protein per 0.5 ml CoIP buffer. Samples were incubated over night at 4°C with RyR2 specific antibodies (rabbit anti-RyR2 (Sigma, HPA020028); mouse anti-RyR2 (Thermo, MA3-916)) or unspecific IgG antibodies (rabbit IgG (Millipore, 12-370); mouse IgG (Millipore, 12-371)) as negative control. The next day, samples were mixed with 900 µg Dynabeads Protein G (10007D, Thermo) and incubated at 4°C for 2 hours on an overhead shaker. Samples were washed three times for 10 min with ice-cold CoIP buffer. For elution, the beads were incubated with 2x sample buffer containing β-mercaptoethanol for 10 min. After SDS-PAGE, proteins were transferred onto PVDF membranes. The membrane was cut and the individual pieces were incubated with primary antibodies over night at 4°C. Epac1-JNC was detected via YFP (Thermo, CAB4211). For detailed antibody information please refer to **Supplementary Table 2**.

References

1. Brandenburg S, Kohl T, Williams GS, Gusev K, Wagner E, Rog-Zielinska EA, Hebisch E, Dura M, Didie M, Gotthardt M, Nikolaev VO, Hasenfuss G, Kohl P, Ward CW, Lederer WJ and Lehnart SE. Axial tubule junctions control rapid calcium signaling in atria. *J Clin Invest*. 2016;126:3999-4015.
2. Zhang L, Kelley J, Schmeisser G, Kobayashi YM and Jones LR. Complex formation between junctin, triadin, calsequestrin, and the ryanodine receptor. Proteins of the cardiac junctional sarcoplasmic reticulum membrane. *J Biol Chem*. 1997;272:23389-97.
3. Wagner E, Brandenburg S, Kohl T and Lehnart SE. Analysis of tubular membrane networks in cardiac myocytes from atria and ventricles. *J Vis Exp*. 2014:e51823.
4. Berisha F, Gotz K, Wegener JW, Brandenburg S, Subramanian H, Molina CE, Rueffer A, Petersen J, Bernhardt A, Girdauskas E, Jungen C, Pape U, Kraft AE, Warnke S, Lindner D, Westermann D, Blankenberg S, Meyer C, Hasenfuss G, Lehnart SE and Nikolaev VO. cAMP Imaging at Ryanodine Receptors Reveals beta2-Adrenoceptor Driven Arrhythmias. *Circ Res*. 2021.
5. Calebiro D, Nikolaev VO, Gagliani MC, de Filippis T, Dees C, Tacchetti C, Persani L and Lohse MJ. Persistent cAMP-signals triggered by internalized G-protein-coupled receptors. *PLoS Biol*. 2009;7:e1000172.
6. Yuan Q, Fan GC, Dong M, Altschafl B, Diwan A, Ren X, Hahn HH, Zhao W, Waggoner JR, Jones LR, Jones WK, Bers DM, Dorn GW, 2nd, Wang HS, Valdivia HH, Chu G and Kranias EG. Sarcoplasmic reticulum calcium overloading in junctin deficiency enhances cardiac contractility but increases ventricular automaticity. *Circulation*. 2007;115:300-9.
7. Lehnart SE, Wehrens XH, Reiken S, Warrier S, Belevych AE, Harvey RD, Richter W, Jin SL, Conti M and Marks AR. Phosphodiesterase 4D deficiency in the ryanodine-receptor complex promotes heart failure and arrhythmias. *Cell*. 2005;123:25-35.
8. Treves S, Vukcevic M, Maj M, Thurnheer R, Mosca B and Zorzato F. Minor sarcoplasmic reticulum membrane components that modulate excitation-contraction coupling in striated muscles. *J Physiol*. 2009;587:3071-9.
9. Brandenburg S, Pawlowitz J, Eikenbusch B, Peper J, Kohl T, Mitronova GY, Sossalla S, Hasenfuss G, Wehrens XH, Kohl P, Rog-Zielinska EA and Lehnart SE. Junctophilin-2 expression rescues atrial dysfunction through polyadic junctional membrane complex biogenesis. *JCI Insight*. 2019;4.
10. Brandenburg S, Pawlowitz J, Fakuade FE, Kownatzki-Danger D, Kohl T, Mitronova GY, Scardigli M, Neef J, Schmidt C, Wiedmann F, Pavone FS, Sacconi L, Kutschka I, Sossalla S, Moser T, Voigt N and Lehnart SE. Axial Tubule Junctions Activate Atrial Ca(2+) Release Across Species. *Front Physiol*. 2018;9:1227.
11. Borner S, Schwede F, Schlipp A, Berisha F, Calebiro D, Lohse MJ and Nikolaev VO. FRET measurements of intracellular cAMP concentrations and cAMP analog permeability in intact cells. *Nat Protoc*. 2011;6:427-38.
12. Yan P, Acker CD, Zhou WL, Lee P, Bollensdorff C, Negrean A, Lotti J, Sacconi L, Antic SD, Kohl P, Mansvelder HD, Pavone FS and Loew LM. Palette of fluorinated voltage-sensitive hemicyanine dyes. *Proc Natl Acad Sci U S A*. 2012;109:20443-8.
13. Scardigli M, Crocini C, Ferrantini C, Gabbrielli T, Silvestri L, Coppini R, Tesi C, Rog-Zielinska EA, Kohl P, Cerbai E, Poggesi C, Pavone FS and Sacconi L. Quantitative assessment of passive electrical properties of the cardiac T-tubular system by FRAP microscopy. *Proc Natl Acad Sci U S A*. 2017;114:5737-5742.
14. Crocini C, Ferrantini C, Scardigli M, Coppini R, Mazzoni L, Lazzeri E, Pioner JM, Scellini B, Guo A, Song LS, Yan P, Loew LM, Tardiff J, Tesi C, Vanzi F, Cerbai E, Pavone FS, Sacconi L and Poggesi C. Novel insights on the relationship between T-tubular defects and contractile dysfunction in a mouse model of hypertrophic cardiomyopathy. *J Mol Cell Cardiol*. 2016;91:42-51.
15. Fakuade FE, Steckmeister V, Seibertz F, Gronwald J, Kestel S, Menzel J, Pronto JRD, Taha K, Haghighi F, Kensah G, Pearman CM, Wiedmann F, Teske AJ, Schmidt C, Dibb KM, El-Essawi A, Danner BC, Baraki H, Schwappach B, Kutschka I, Mason FE and Voigt N. Altered atrial cytosolic calcium handling contributes to the development of postoperative atrial fibrillation. *Cardiovasc Res*. 2021;117:1790-1801.